Classical transport of electrons through magnetic barriers

I. S. Ibrahim, V. A. Schweigert,* and F. M. Peeters†

Departement Natuurkunde, Universiteit Antwerpen (UIA), Universiteitsplein 1, B-2610 Antwerpen, Belgium

We investigate the magnetoresistance of a two-dimensional electron gas (2DEG) in the presence of wide (width of order μm) magnetic barriers. A Poisson-like equation is solved numerically from which we obtain the 2D electrostatic potential, electric field, and current distribution in the 2DEG. We found that most of the electrons are injected at the edge of the magnetic barrier and most of the potential drop takes place in the barrier region. Major features of a recent magnetoresistance experiment by Leadbeater *et al.* [Phys. Rev. B **52**, R8 629 (1995)] on single and double faceted structures can be explained by our classical approach. The positive background magnetoresistance and the nonlocal Hall effect are reproduced. These results allow one to disentangle classical and quantum features of the experimental results. [S0163-1829(97)03036-1]

I. INTRODUCTION

Subjecting two-dimensional electron gas (2DEG) systems to different physical environments has greatly improved our understanding of these systems and has led to the observation of several remarkable phenomena such as the integer and the fractional quantum Hall effects,[1] conductance quantization in quantum point contacts,[2] the Aharonov-Bohm effect, and the Weiss oscillations to mention just a few. Recently, an increasing amount of effort is devoted to the experimental and theoretical investigation of the behavior of the 2DEG under the influence of a nonhomogeneous magnetic field.[3] Such nonhomogeneous magnetic field profiles can be produced, e.g., by depositing lithographic patterned superconducting or ferromagnetic films on top of a heterojunction.

Recently, Leadbeater *et al.*[4] reported an alternative technique to produce effective spatially varying magnetic fields of much larger strength and gradients than could be obtained by lithographic patterned superconducting or ferromagnetic films. They constructed a nonplanar 2DEG which was fabricated by growth of a GaAs/(AlGa)As heterojunction on a wafer prepatterned with facets at 20° to the substrate. Applying a uniform magnetic field (B) produces a spatially nonuniform field component perpendicular to the 2DEG (see inset of Fig. 2). With the field in the plane of the substrate an effective magnetic barrier is created located at the facet. The resistance measured across such an etched facet showed oscillations which are periodic in $1/B$, and which are on top of a positive magnetoresistance background which increases quadratically with the magnetic field for small B and quasi-linearly in B for large B.

In the present paper we demonstrate that the large positive magnetoresistance is a classical effect resulting from the particular potential distribution in the sample as a consequence of the nonhomogeneous magnetic field distribution which is well described by a Poisson-like equation with the appropriate boundary conditions. The small oscillations on top of this positive magnetoresistance background are a quantum effect and are in fact Shubnikov–de Haas oscillations.

For the experimental traces shown in Figs. 2 and 3 of Ref. 4 we give in Fig. 1 a schematic top view of the experimental

system for later reference. In this figure the probes 1 and 8 are current probes and the probes numbered 2–7 and 9–14 are voltage probes. The nonzero magnetic field region (i.e., the facet region) is the gray-shaded region in the middle of the Hall bar. The relevant distances used in the experiment of Ref. 4 are $L>920$ μm, $W=40$ μm, $S=3$ μm, $d_1=200$ μm, $d_2=255$ μm, $d_3=10$ μm, and $d_4=220$ μm. Note also that there is an offset on the experimental curves in Fig. 3 of Ref. 4, and all the traces for R_{11-10}, R_{5-6}, ... R_{13-12} are shifted by 50 Ω to prevent overlap with R_{4-12}. Consequently, the zero field resistances are $R_{2-3}=260$ Ω, $R_{3-4}=R_{13-12}=330$ Ω, and $R_{5-6}=R_{11-10}=220$ Ω.[5]

The paper is organized as follows. In Sec. II we present our theoretical model. Section III contains the results for the case of a single facet, i.e., a single magnetic barrier. The effect of placing such barriers in series is investigated in Sec. IV. Concluding remarks are presented in Sec V.
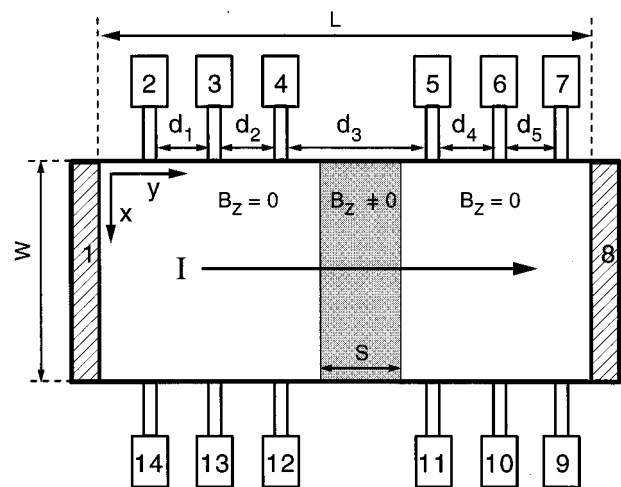

FIG. 1. A schematic top view of the experimental system of Ref. 4 illustrating the geometry and the different probes. The gray-shaded region is the facet region. $L>920$ μm, $W=40$ μm, $S=3$ μm, $d_1=200$ μm, $d_2=255$ μm, $d_3=10$ μm, $d_4=220$ μm.

II. THEORETICAL MODEL

To explain, quantitatively, the main features of the experimental measurements of Ref. 4, namely, the smooth background of the magnetic field dependence of the resistance, we will rely on a classical model. The 2DEG situated in the (x,y) plane is bounded by the edges of the Hall bar of Fig. 1 where a small part of the 2DEG, represented by the gray-shaded region in Fig. 1, is subjected to a perpendicular magnetic field which is in the z direction. The $B_z \neq 0$ region corresponds to the facet region in the experimental system, i.e., $B_z = B \sin(\theta)$, $\theta = 20°$ is the facet angle, and B is the externally applied magnetic field in the plane of the substrate. In order to calculate the spatial distribution of the electrostatic potential, the electric field and the current density, we start with the following system of Maxwell equations in the plane of the 2DEG:

$$\nabla \cdot \mathbf{E} = 4\pi\rho, \tag{1}$$

$$\nabla \times \mathbf{B} - \frac{\partial \mathbf{E}}{\partial t} = \frac{4\pi}{c}\mathbf{J}, \tag{2}$$

$$\nabla \times \mathbf{E} + \frac{\partial \mathbf{B}}{c\,\partial t} = 0. \tag{3}$$

For our purposes Eqs. (1) and (2) can be combined into a single continuity equation, which expresses charge conservation, by taking the time derivative of the first and the gradient of the second

$$\nabla \cdot \mathbf{J} + \partial\rho/\partial t = 0. \tag{4}$$

In addition to the Lorentz force, a single electron in the sample moves under the influence of a dissipative or a resistive force due to various scattering mechanisms. This force is proportional to the average electron velocity and is given by $m^*\mathbf{v}/\tau$, where τ is the transport relaxation time which is related to the measured mobility $\mu_e = e\tau/m^*$ of the sample. Then the net force exerted on the electron is

$$m^*\frac{d\mathbf{v}}{dt} = e\left(\mathbf{E} + \frac{\mathbf{v}}{c}\times\mathbf{B}\right) - \frac{m^*\mathbf{v}}{\tau}, \tag{5}$$

which, in essence, is the Langevin equation for a Brownian particle. In the steady state all time derivatives are set to zero. When Eq. (5) is multiplied by the charge density it can be written in the form of Ohm's law but where now the conductivity is a spatially dependent tensor due to the presence of the nonhomogeneous magnetic field. We are left with the following set of equations:

$$\nabla \times \mathbf{E} = 0, \tag{6}$$

$$\nabla \cdot \mathbf{J} = 0, \tag{7}$$

$$\mathbf{J} = \sigma\mathbf{E}. \tag{8}$$

Writing the electric field as the gradient of a potential, i.e., $\mathbf{E} = -\nabla\phi$ the above system of equations reduces to the following 2D elliptic partial differential equation for the electrical potential ϕ:

$$\nabla \cdot [\sigma(x,y)\nabla\phi(x,y)] = 0, \tag{9}$$

where $\sigma(x,y)$ is a spatial dependent conductivity tensor. For a homogeneous system and in the abscence of a magnetic field $\sigma(x,y) = $ const, and this equation reduces to the Laplace equation. In our case the conductivity tensor is no longer constant due to the presence of the finite magnetic barrier: $\sigma(x,y) = \alpha[\sigma_{ij}]$, where $\alpha = \sigma_0/[1 + (\mu_e B_z)^2]$ with the components $\sigma_{xx} = \sigma_{yy} = 1$ and $\sigma_{xy} = -\sigma_{yx} = \mu_e B_z$ where $\sigma_0 = n_s e \mu_e$ is the Drude conductivity and $B_z = 0$ outside the facet. The 2D partial differential equation is cast into a finite-difference form and solved numerically using the accelerated Gauss-Seidel iteration scheme with the boundary conditions $\phi(x,0) = 0$ and $\phi(x,L) = V_0$ (L is the length of the sample and V_0 is the applied voltage) and the condition that no current can flow out the sides of the sample, i.e., $j_x = 0$ for $x = 0$, and $x = W$. The distances are normalized by the width of the sample (typically $W = 40$ μm taken along the x axis) and voltages are normalized by the total voltage drop between the current probes 1 and 8. The magnetoresistance between any two points a and b along one side of the sample is given by $R = V_{ab}/I_{cd}$, with the voltage drop $V_{ab} = \phi(x,b) - \phi(x,a)$, and the total current flowing normal to the facet is obtained through $I_{cd} = \int_c^d j_y(x,y)dx$, where c and d are any two points on the opposite sides of the sample. The Hall resistance at a distance y along the sample length is given by $R_H = V_H/I_{cd}$, where $V_H = \phi(W,y) - \phi(0,y)$. In our numerical analysis we used $\sigma_0 = 1/(53.146\ \Omega)$ as obtained from the experimentally measured resistance in Ref. 4.

III. RESULTS FOR A SINGLE MAGNETIC BARRIER

In Fig. 2 we show both the experimental (solid curve) and the theoretical (dashed curve) traces for the magnetoresistance R_{4-5} for the case of a single facet. For the experimental trace shown in the figure the current is kept constant and the voltage probes are situated 10 μm apart across the facet and the current probes are more than 900 μm apart. For the theoretical curve the voltage difference between probes (4 and 5) is maintained constant as a boundary condition and the current is allowed to vary with the magnetic field, therefore it is sufficient to take the length of the sample L to be 10 μm (i.e., the distance between the voltage probes 4 and 5) and consequently $L = 0.25$ is the length of our sample in units of $W = 40$ μm. The numerical computations were done using a uniform grid (i.e., equally spaced grid points in each direction x and y) since in this particular case the sample is not very long. In Fig. 2 it is seen that apart from the Shubnikov–de Haas (SdH) oscillations, which result from the quantizing effect of the magnetic field at low temperature, the theoretical curve accounts nicely for the overall behavior of the magnetoresistance. The experimental curve is slightly asymmetric around $B = 0$, which is due to the fact that the voltage probes are not exactly equidistant from the facet as will be explained below. The classical origin of the positive magnetoresistance was confirmed experimentally where it was found that it persists even for temperatures above 100 K. Note that the experimental configuration is effectively a two terminal measurement where the measured resistance is determined by the Hall resistance as well as the magnetoresistance. For small B fields the Hall resistance is
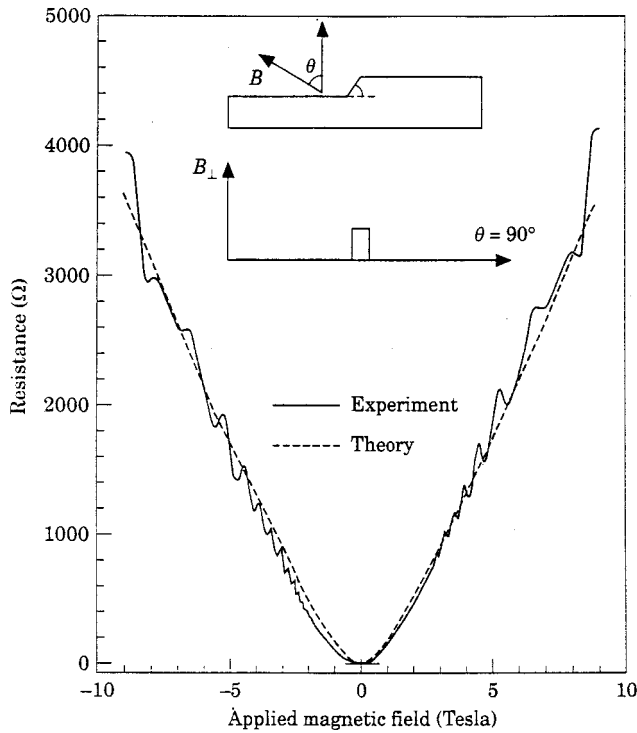
FIG. 2. The magnetoresistance R_{4-5} as a function of the applied magnetic field. The inset shows a schematic side view of the facet plane making an angle of $20°$ to the substrate, together with the magnetic field profile perpendicular to the 2DEG.

small and thus the resistance is determined by the magnetoresistance and is consequently quadratic in B. For larger magnetic fields a quasilinear behavior of the resistance as a function of B is found which is due to the fact that now the Hall resistance mainly limits the current.

The theoretical electric potential distribution in the sample is shown in Fig. 3 for an applied magnetic field of
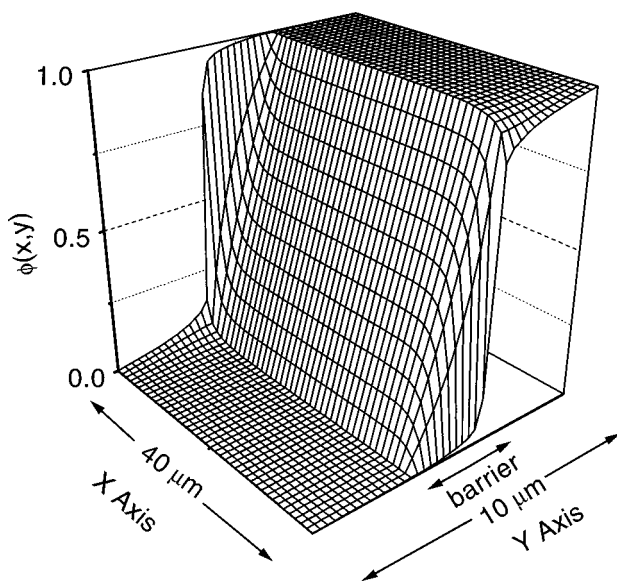

FIG. 3. The potential distribution in the sample for $B = -2$ T which results into $B_z = -0.684$ T.
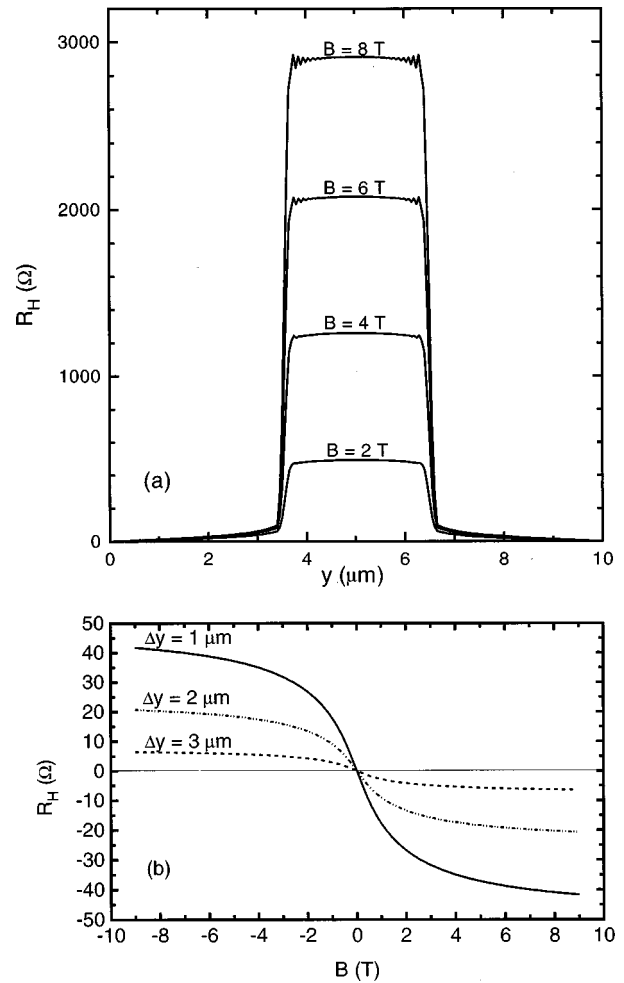

FIG. 4. (a) The Hall resistance calculated across the sample as a function of the longitudinal distance along the sample for different values of the applied magnetic field. (b) The Hall resistance in the $B_z = 0$ region as a function of the magnetic field for different distances Δy from the boundary of the magnetic barrier. The parameters are the same as those used in Figs. 2 and 3.

$B = -2$ T, which gives $B_z = -2\sin(20°) = -0.6840$ T. Notice that almost all the potential drop takes place across the magnetic barrier. In the barrier region and just outside it there is a voltage difference between the edges of the sample (i.e., across the x axis), which is nothing else than a spatially dependent Hall voltage. This is in accord with the concept that the ($B_z = 0$ regions) can be thought of as extended high mobility contacts to a short and wide Hall bar (the facet region) which tends to short out most of the voltage immediately outside the facet region. Particularly interesting is the development of the Hall voltage between the opposite edges of the facet. This becomes very small but nonzero outside the facet region and gives a steep increase of the Hall potential profile at the edges of the $B_z \neq 0$ region which is reminiscent of the potential profile investigated experimentally and theoretically in Refs. 6 and 7 in a conventional Hall bar under the conditions of the quantum Hall regime and in the middle of a plateau in the Hall resistance (see Fig. 3). In Fig. 4(a) we show the Hall resistance for different magnetic barrier strengths and along the length of the sample. Notice that $R_H \neq 0$ in the $B_z = 0$ regions. This is made more visible in Fig. 4(b), where we show the Hall resistance at different
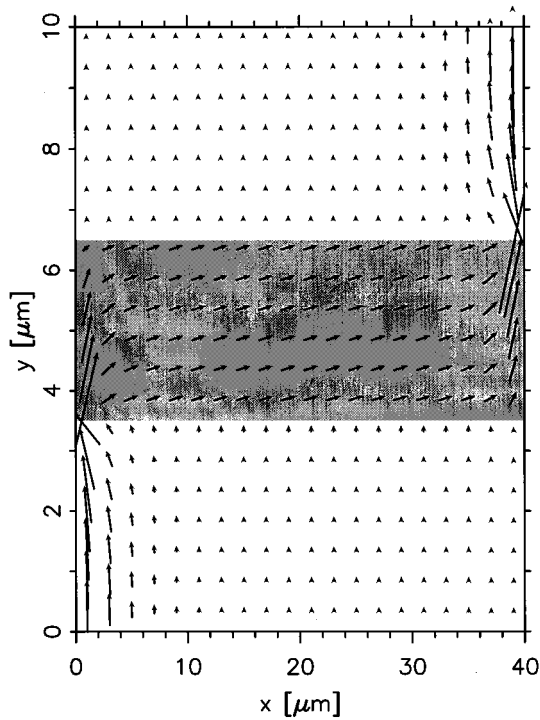
FIG. 5. The current flow in the sample for $B = -2$ T. The magnetic barrier region is gray shaded. The local magnitude and direction of the current is proportional to the magnitude and direction of the arrows, respectively.

distances Δy from the boundary of the magnetic barrier. This is an example of a nonlocal Hall resistance which in the present case is a classical effect. The small oscillation in Fig. 4(a) near the edge of the magnetic barrier are due to the finite size of the grid used in our numerical calculation.

The spatial distribution of the components of the electric field are obtained as follows: $E_x = -\partial\phi(x,y)/\partial x$ and $E_y = -\partial\phi(x,y)/\partial y$. From Fig. 3 it is clear that both components are very small outside the barrier region. Inside the magnetic barrier, E_x becomes very large close to the edges especially at the diagonally opposite corners and vanishingly small in the middle where E_y is finite and more uniform, singular at the diagonally opposite corners and very small at the other two corners. Accordingly, the largest part of the current will enter the magnetic barrier region from the corner where both electric field components are large and exit the barrier from the diagonally opposite corner. Once inside the barrier region the guiding center of the electron cyclotron orbits will drift along the equipotential lines (see Fig. 3) according to the $\mathbf{E} \times \mathbf{B}$ drift with velocity $\mathbf{v}_{\text{drift}} = -(\nabla\phi \times \mathbf{B})/B^2$. Electrons entering or exiting the small regions of the corners of the barrier will have large velocities, which are proportional to the electric field at these locations, to account for current conservation. There are larger number of electrons drifting with slow and uniform velocities in the middle of the barrier where the electric field is smaller and more uniform. This picture is graphically represented in Fig. 5 where we show the calculated results for the current distribution $\mathbf{J}(x,y) = -\sigma(x,y)\nabla\phi(x,y)$ corresponding to the experimental situation of Fig. 3. Notice that even well outside the barrier the current distribution is already modified by the presence of the magnetic field barrier in the facet region

and it is concentrated closer to the edges of the sample. At the diagonally opposite corners it is strongly peaked. These results for the field and current distribution are consistent with those of Ref. 8 which were calculated for a conventional Hall geometry in the case of very low aspect ratio.

It is evident from the potential distribution (see Fig. 3) or equivalently the spatial distribution of the electric field components that there is a linear excess charge distribution (induced by the magnetic barrier) with a δ function profile along the y axis at the interfaces between the magnetic-nonmagnetic field regions due to the finite discontinuity of the normal component of the electric field E_y at the interfaces. The linear excess charges have opposite signs at the two interfaces. This charge profile can be obtained by taking the second partial derivative of the calculated potential distribution in both directions x and y, i.e., $\lambda(x,y) = \nabla^2\phi(x,y)$. These results were recently also obtained in Ref. 9 by the complex variable method of conformal mapping. It is possible to obtain an analytical expression for the induced charge at one (for $y = a$) of the magnetic-nonmagnetic interfaces in terms of the electric field components at the interface,

$$\lambda(x,y) = \frac{\mu_e B_z}{1 + (\mu_e B_z)^2}\{[1 - (\mu_e B_z)^2]E_x + 2\mu_e B_z E_y\}$$
$$\times \delta(y - a). \tag{10}$$

At the other interface, i.e., at $y = b$, the induced charge has the same form but with $\delta(y-a)$ replaced by $-\delta(y-b)$.

In Fig. 6 we investigate the effect of the sample length on the resistance (full and dash-dot-dot curves) where the voltage probes were taken the same as the current probes i.e., $L = d$. Note that when the magnetic field is uniform over the whole sample, i.e., $L = d = 3$ μm (dash-dot-dot curve) the resistance equals the magnetoresistance which is independent of the magnetic field and which is a result expected from a classical calculation. Notice also that the resistance slightly increases with increasing length of the sample (compare dotted curve with full curve). The reason is that there are now larger $B_z = 0$ regions which give a small contribution to the resistance. Next we investigated the effect of temperature, which is simulated by reducing the mobilty. In the present case of a low temperatue mobility of $\mu_e = 245\,000$ cm^2/V s a reduction of μ_e by a factor of 10 is achieved in the GaAs/Al$_x$Ga$_{1-x}$As heterostructure by increasing the temperature to $T \approx 90$ K. The result for this situation is given by the dash-dotted curve in Fig. 6. Notice that the B^2 behavior extends now up to larger B values. The positive magnetoresistance is still clearly present at these modeled high temperatures allowing the practical use of the present device as a magnetometer.[10] Notice that over the B region : $0 \rightarrow 8$ T the magnetoresistance curve still increases by a factor of 10 which compares to a factor of 276 for $T = 4.2$ K.

In order to calculate the other resistance traces shown in Fig. 3 of Ref. 4 we have to use the actual length of the experimental sample $L = 920$ μm or $L/W = 23$. With this sample length it is necessary to use a nonuniform grid along the length of the sample (y direction) in order to be able to have sufficient grid points within the magnetic barrier region which is $S/W = 0.075$ long. The current probe 1 has been set
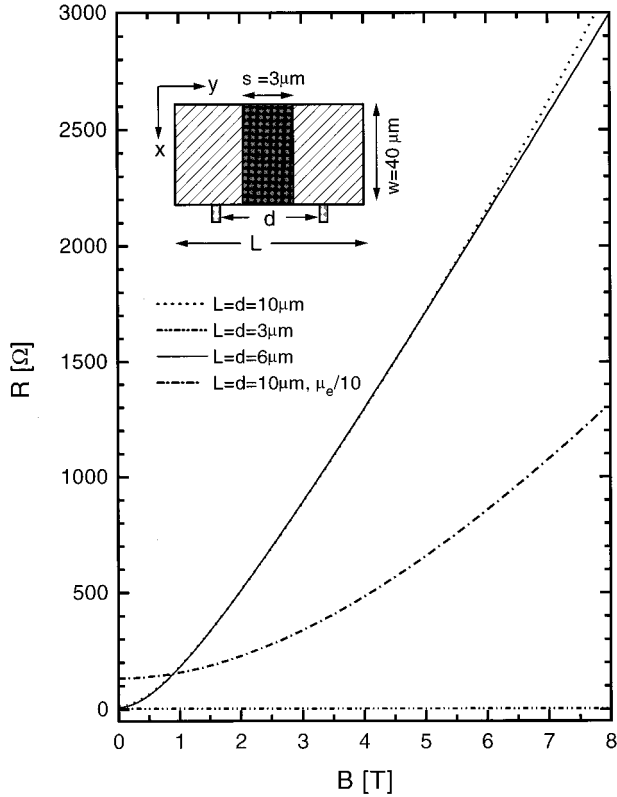
FIG. 6. The resistances R_{4-5} as a function of the applied magnetic field for different lengths of the sample. For the dash-dotted curve the mobility is reduced by a factor of 10 simulating the effect of a higher temperature.
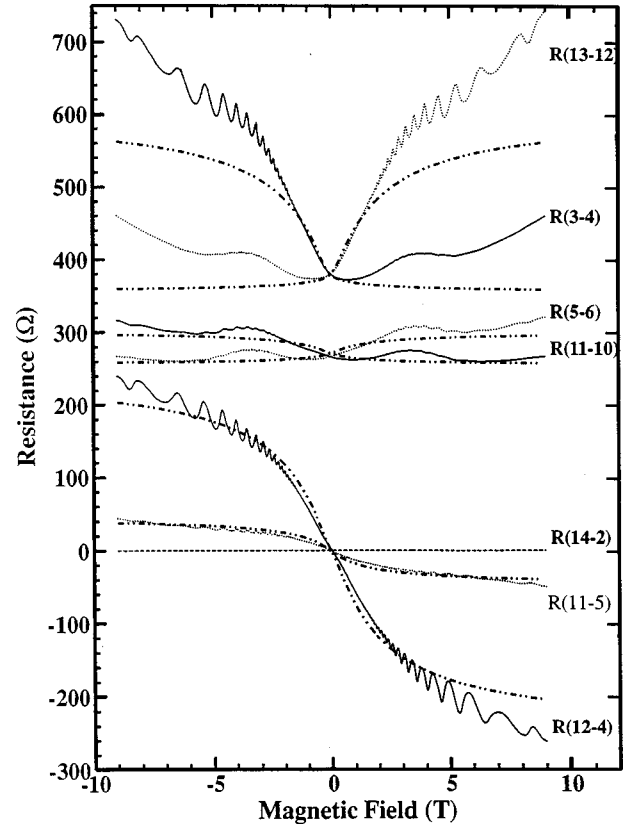

FIG. 7. The resistance as a function of magnetic field. The experimental traces are the solid and the dotted curves. Our results are the dash-dot-dot curves obtained for asymmetrically placed probes (see text).

to have the same distance from the center of the facet as voltage probe 2 (i.e., 460 μm) and current probe 8 at the same distance as probe 7 which is also at 460 μm from the center of the facet. For the other probes we used the distances given in the caption of Fig. 1. The convergence of the nonuniform grid calculation with $L = 920$ μm as compared to the previous uniform grid with only $L = 10$ μm is much slower due to the large length of the sample. As a test we have verified that the results for R_{4-5} for the long sample can be brought to good agreement with that of the short one (dashed curve in Fig. 2) by reducing the tolerance and increasing the number of iterations. In Fig. 7 we show our numerical results (dash-dot-dot curves) together with the resistances measured (solid and dotted curves) in Ref. 4. First, observe that all the (a) symmetries of the experimental curves resulting from the sign reversal of the magnetic field are reproduced. Second, theoretically the following relations between the resistances hold: $R_{13-12} = R_{5-6}$, $R_{3-4} = R_{11-10}$, and $R_{4-12} = R_{5-11}$ if the probes are symmetrically placed from the center of the facet and if they have the same distances between the voltage probes. Looking at the experimental traces in Figs. 2 and 7 one can conclude that the probes are not symmetrically placed from the center of the facet region. For instance, in Fig. 2 the experimental trace for R_{4-5} exhibits a difference of approximatly 200 Ω between the $B = +9$ T and $B = -9$ T results. Also the large difference in magnitude between R_{4-12} and R_{5-11} and the fact that the quantum oscillations are more pronounced in R_{4-12} than in R_{5-11} can be attributed to the same cause implying

that R_{4-12} is less than a scattering length away from the facet ($l_s = \tau v_f = 2.76$ μm), where electrons still carry a substantial memory effect from the nonzero magnetic field region. Thus probes 5 and 11 are probably more than l_s away from the facet region and the electrons are in better equilibrium with the rest of the 2DEG in the zero field region. These facts can also explain the large asymmetry observed in the experimental traces between R_{3-4} and R_{13-12} having clear quantum oscillations and the much less pronounced asymmetry and the almost absence of quantum oscillation between the other two traces R_{5-6} and R_{11-10}. In fact, our numerical results (dash-dot-dot curves) in Fig. 7 are obtained for the following probe positions: probes 12 and 4 are 0.01 μm away from the facet, and probes 11 and 5 are 6.99 μm away from the facet, keeping the distance between probes 4 and 5 fixed, i.e., $d_3 = 10$ μm. It is obvious that our results are in good agreement with all the experimental traces except in the high magnetic field regions for traces R_{13-12} and R_{3-4} for reasons that are not clear to us for the moment. When the probes are symmetrically placed on both sides of the magnetic barrier then the traces R_{11-5} and R_{12-4} coincide with a value of 55Ω at -9 T, and the resistaces at 9 T of R_{13-12} and R_{3-4} are 418 Ω and 363 Ω, respectively.

The problem of low aspect ratio Hall devices in a homogeneous magnetic field was studied earlier in the context of applications for magnetic sensors (see, e.g., Ref. 10 and references therein). The longitudinal magnetoresistance of a simple rectangular plate is given by $R(B) = R(B$
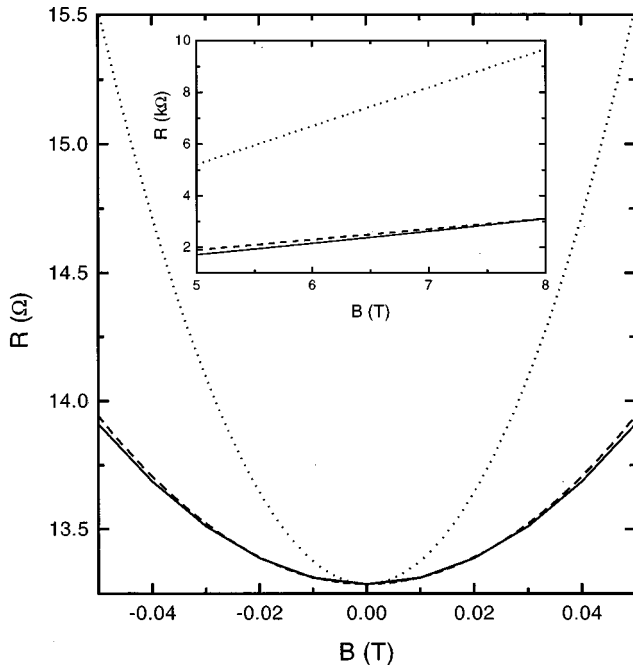
FIG. 8. The longitudinal resistance for small B fields (inset for large B fields). Our results are (solid curve) compared to those given by the limiting expressions of Ref. 10 (dotted curves). The results from the limiting expressions using an effective barrier width are given by the dashed curves.

$=0)R_g(\theta,L/W)$, where θ is the Hall angle, i.e., $\tan(\theta)=\mu_e B$. In the limit $L/W\rightarrow0$ the so called geometrical contribution $R_g(\theta,L/W)$ can be obtained analytically in two extreme cases: (i) (limit $\theta\rightarrow0$, i.e., low magnetic field) $R_g=1+(1-0.5428L/W)\theta^2$, and (ii) (limit $\theta\rightarrow\infty$, i.e., large mag-
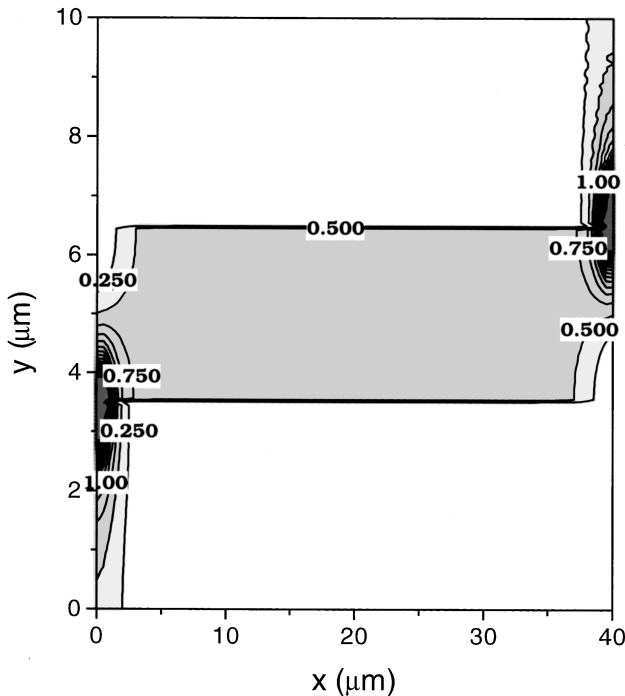

FIG. 9. Contours of the energy dissipation rate for a single magnetic barrier corresponding to Figs. 3 and 5.
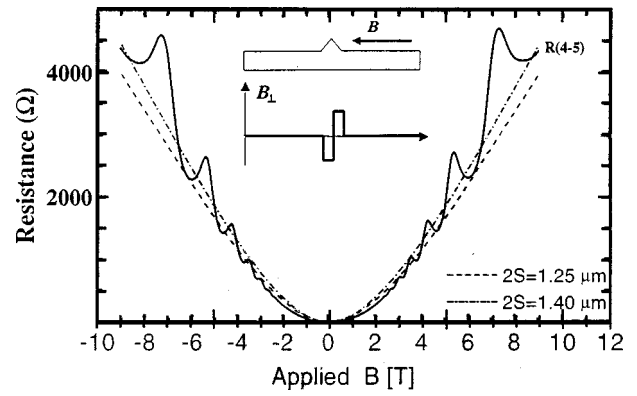

FIG. 10. The magnetoresistance R_{4-5} for the ridge as a function of the applied magnetic field. The theoretical results are for two different values of the ridge width ($2S$). The inset shows a schematic side view of the ridge together with the magnetic field profile perpendicular to the 2DEG.

netic field) $R_g=\{\tan(\theta)+(2/\pi)\ln([1-k]/[2\sqrt{k}])]W/L$, where $k=1-8\exp(-\pi W/(2L^*))\}$. In Fig. 8 we compare the results of these limiting expressions (dotted curves) with our numerical results of Fig. 2 (solid curves) where we used $L=S$ as the length of the Hall bar. It is clear that these expressions strongly overestimate the experimental results over the whole range of the magnetic field. Although these limiting expressions give the correct qualitative B dependence of the resistance in the low ($R\sim B^2$) and high ($R\sim B$)
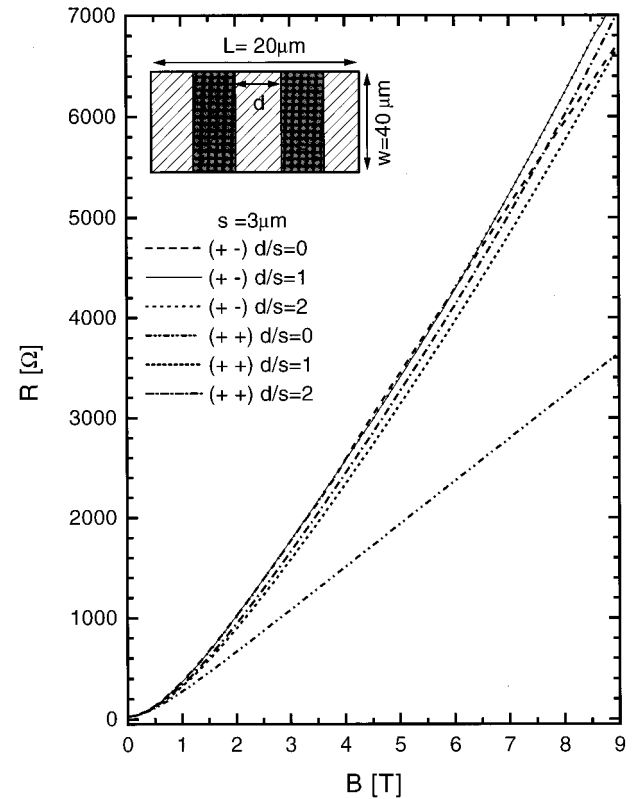

FIG. 11. The magnetoresistance for two magnetic barriers in series (two facets) for different distances between the barriers and for different relative signs of B_z (indicated by the plus/minus signs between brackets).
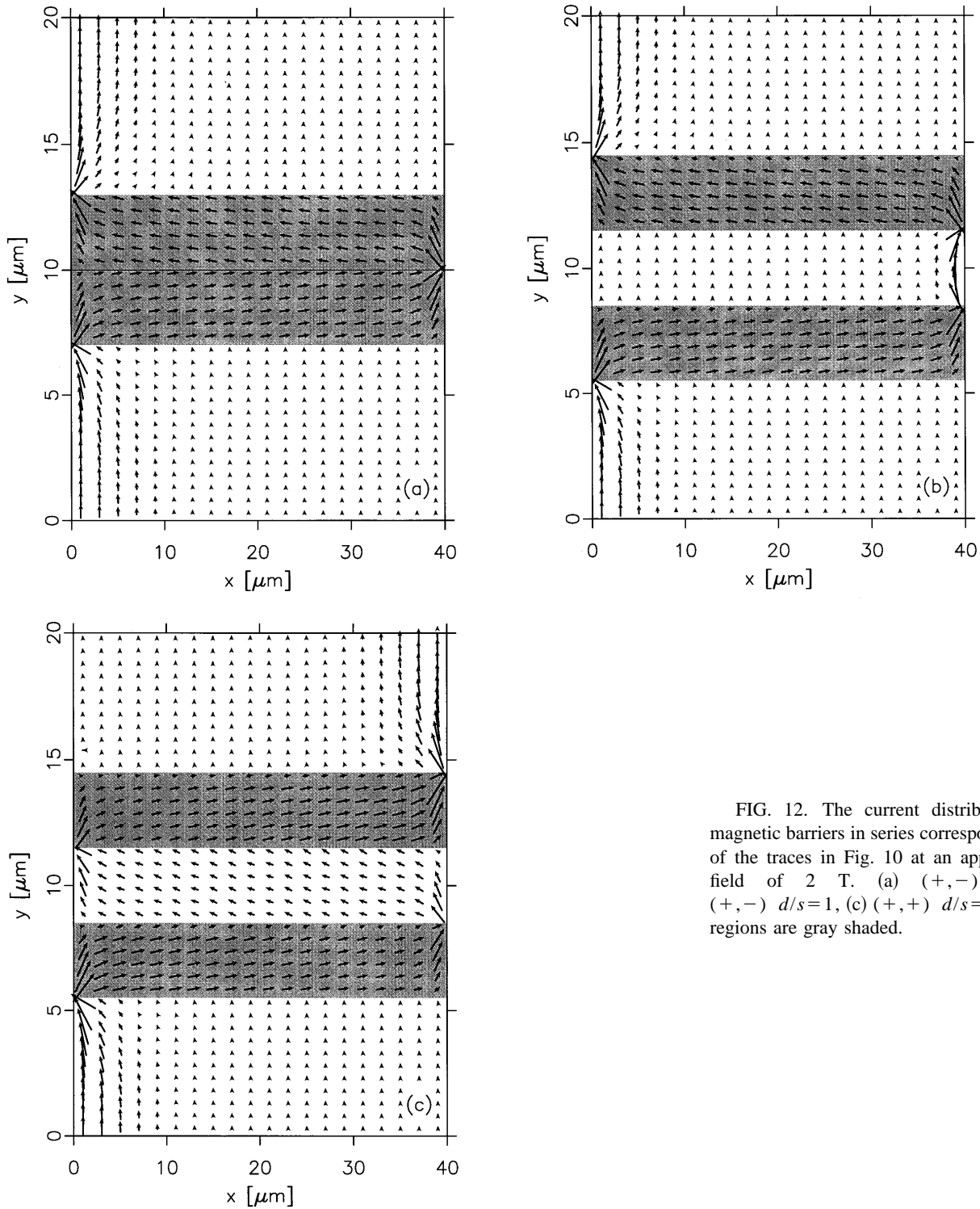
FIG. 12. The current distribution for two magnetic barriers in series corresponding to some of the traces in Fig. 10 at an applied magnetic field of 2 T. (a) $(+,-)$ $d/s=0$, (b) $(+,-)$ $d/s=1$, (c) $(+,+)$ $d/s=1$. The barrier regions are gray shaded.

field limits, they are in fact only order of magnitude estimates for the present case of transport through a magnetic barrier. In order to have also a good quantitative agreement we introduce an effective Hall bar length $L=S^*$, which we obtain by fitting the low magnetic field expression for the magnetoresistance to the solid curve. This is shown by the dashed curve in Fig. 8 for $S^*=53$ μm which compares with a barrier width of $S=3$ μm. The high magnetic field behavior could be fitted approximatly if we use a different length $S^*=12$ μm (see dashed curve in the inset of Fig. 8). This

clearly indicates the very limited applicability of these expressions for our system.

Once we have the current and the electric field distribution in our sample it is possible to calculate the energy dissipation rate $w(x,y)=\mathbf{J}(x,y)\cdot\mathbf{E}(x,y)$. A contour plot of this quantity for a single magnetic barrier corresponding to Figs. 3 and 5 is shown in Fig. 9. Clearly most of the heat is generated near the sides of the sample where the current is concentrated in the zero magnetic field regions, at the current injection and removal corners of the barrier region, and

within the magnetic barrier region itself. At this magnetic field value of 2 T the system is still far from the dissipation-less flow condition of the quantum Hall regime and the Hall angle between the electric field and the current is less than $90°$.

IV. MAGNETIC BARRIERS IN SERIES

In Ref. 4 a ridge geometry (see top figure of the inset of Fig. 10) was fabricated resulting into two magnetic barriers in series (bottom figure of the inset of Fig. 10), each having the same B_z but with opposite sign. In Fig. 10 both the experimental (solid) trace and the theoretical (dash-dotted and dashed) curves are shown. The experimental trace was claimed to be for $2S = 1$ μm base length of the ridge (in Ref. 4 it is noted that the etch depth for a ridge is less than the depth of the regrown material, which may produce some planarization during regrowth), while for the theoretical curves we found that a larger base length gives closer agreement with experiment. The numerical computations were done in the same manner as for the single facet discussed in the preceeding section maintaining a constant potential difference between voltage probes (4)–(5). Notice that with this renormalization of the width of the magnetic barrier we obtan rather good agreement for the positive magnetoresistance part of the experimental curves. The oscillatory part in the experimental curves are again due to quantum effects.

Next we consider the more general case of two magnetic barriers in series. This can be realized experimentally by producing a ridge with a flat top which is equivalent to introducing a zero magnetic field region between the two facets. In Fig. 11 we show the magnetoresistance for such a double barrier structure where we varied (1) the distance (d) between the barriers, and (2) the relative sign of the magnetic field in the two magnetic barriers. The difference between these curves can be understood in terms of the different current paths followed by the electrons which are shown in Figs. 12(a)–12(c). From Figs. 11 and 12 we conclude that in high magnetic fields ($R \sim B$) the current is effectively injected and removed from the extremely narrow regions of the diagonally opposite corners of the facet and in the case of barriers with equal direction of the magnetic field the bulk part of the magnetoresistance is proportional to the number of pairs of injection and removal points of current. For the case of two separate barriers with the same sign of B_z the magnetoresistance at high magnetic fields is almost twice that of a single barrier and consequently we find classically that the magnetoresistance of multiple barriers is additive [compare dash-dot-dot curve, i.e., $(+,+)$ $d/s = 0$, with short dashed curve, i.e., $(+,+)$ $d/s = 1$ in Fig. 10]. For not too large magnetic fields (the $R \sim B^2$ region) the current path spreads across the magnetic-nonmagnetic interface and consequently the current path is shorter, leading to a smaller magnetoresistance, and the simple rule of addition of resistances in series is no longer valid. For barriers in series with opposite direction of the B_z field the situation is different [compare Fig. 12(b) with Fig. 12(c)]. The removal point of current from the first barrier is at the same side of the sample as the injection point of the current into the second barrier and consequently the resistance is not sensitive to the value of the separation between the two barriers. This is also clearly visible in Fig. 11
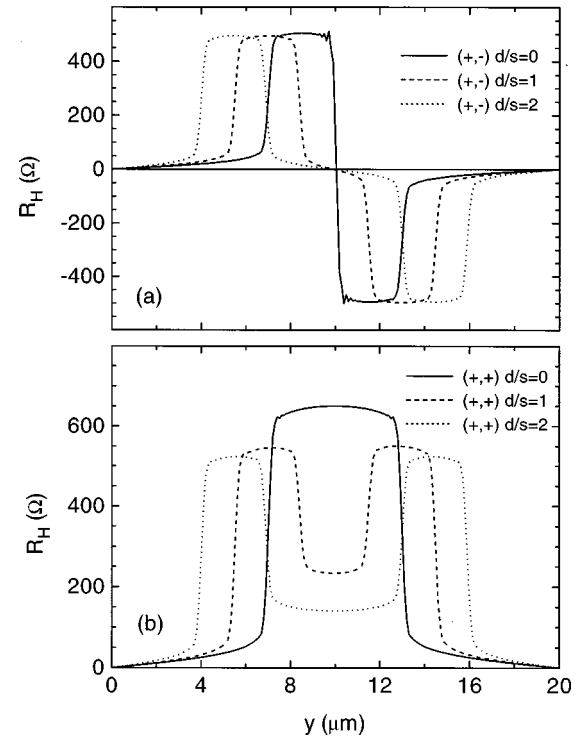

FIG. 13. The Hall resistance along the sample for two magnetic barriers in series for different distances between the barriers and for (a) opposite relative signs of B_z, and (b) equal signs of B_z in the two magnetic barriers. The applied magnetic field is 2 T.

where one should compare the dashed curve, i.e., $(+,-)$ $d/s = 0$, with the thin solid curve, i.e., $(+,-)$ $d/s = 1$.

In Fig. 13 we show the Hall resistance as a function of the distance along the sample (along the y direction). It is large and almost constant across each barrier and drops steeply to small but nonzero values in the zero magnetic field region as explained earlier. When the two barriers have the same sign [Fig. 13(b)] and the distance between them is nonzero there is a finite Hall voltage across the region between the two barriers (the $B_z = 0$ region). This is because the current has to travel to the diagonally opposite corner to enter the second barrier [see Fig. 12(c)] and hence there is a finite electric field component along the current path in this region which becomes smaller as the distance between the two barriers is increased. This is not the case, however, when the barriers have opposite sign because the current comes out of the corner of the first barrier and enters the corner of the second barrier at the same side of the sample [see Fig. 12(b)] and there is no electric field build up across the region between the barriers and consequently the Hall voltage is very small. From Fig. 13(b) we notice that the Hall resistance in the magnetic barrier region increases with the width of the magnetic barrier (compare the full curve with the dotted curve). This is only true for the $S/W \ll 1$ situation while for the opposite limit of $S/W \gg 1$ the Hall resistance will be independent of the length of the magnetic barrier.

V. CONCLUDING REMARKS

In conclusion, we have calculated numerically the electrical potential, the electric field, and the current distribution of

40 μm wide Hall bar samples consisting of a single and multiple μm width magnetic barriers using a simple classical model. We found that due to the step like character of the magnetic field nonhomogenuity a self-consistent δ function like charge density is induced at the interface between the magnetic-nonmagnetic field regions which results in the redistribution of the current density in the whole sample and consequently it also influences the electric potential and the electric field profile. In view of the fact that no adjustable parameters were used in our model the agreement of the longitudinal magnetoresistance with experiment is remarkable. Furthermore, all the experimentally observed asymmetries of the magnetoresistance traces between probes placed outside the magnetic barrier regions are explained. From our calculation we found that the asymmetry observed in Ref. 4, being larger between one set of voltage probes than others, is a result of the nonequidistant positioning of these probes from the magnetic barrier. The fact that the experimental nonplaner 2DEG is well modeled by a planar 2DEG makes this regrowth technique a prime candidate for producing large nonhomogeneous magnetic field profiles on a mesoscopic scale.

[*]Permanent address: Institute of Theoretical and Applied Mechanics, Russian Academy of Sciences, Novosibirsk 630090, Russia.

[†]Electronic address: peeters@uia.ua.ac.be

[1]See, e.g., *The Quantum Hall Effects*, T. Chakrabarty and P. Pietiläinen (Springer, Berlin, 1995).

[2]C. W. J. Beenakker and H. van Houten, in *Solid State Physics: Advances in Research and Applications*, edited by H. Ehrenreich and D. Turnbull (Academic, New York, 1991), vol. 44, p. 1.

[3]F. M. Peeters, Phys. World **8**, 24 (1995).

[4]M. L. Leadbeater, C. L. Foden, J. H. Burroughes, M. Pepper, T. M. Burke, L. L. Wang, M. B. Grimshaw, and D. A. Ritchie, Phys. Rev. B **52**, R8629 (1995).

[5]M.L. Leadbeater (private communication).

[6]P. F. Fontein, J. A. Kleinen, P. Hendriks, F. A. P. Blom, J. H. Wolter, H. G. M. Lochs, F. A. J. M. Driessen, L. J. Giling, and C. W. J. Beenakker, Phys. Rev. B **43**, 12 090 (1991).

[7]A. H. MacDonald, T. M. Rice, and W. F. Brinkman, Phys. Rev. B **28**, 3648 (1983).

[8]R. W. Rendell and S. M. Girvin, Phys. Rev. B **23**, 6610 (1981).

[9]S. M. Badalian, I. S. Ibrahim, and F. M. Peeters, in the *Proceedings of the International Conference on High Magnetic Fields in Semiconductor Physics*, edited by G. Landwehr and W. Ossau (Springer-Verlag, Berlin, 1997).

[10]J. Heremans, J. Phys. D **25**, 1149 (1993); J. Heremans, D. L. Partin, C. M. Thrush, and L. Green, Semicond. Sci. Technol. **8**, S424 (1993).